P-SV Numerical modelling and AVO of the Cardium conglomerate in the Carrot Creek field of central Alberta, Canada

Ashraf Abdalla

ABSTRACT

This work implements the use of numerical seismic modelling to investigate mode-converted P- to SV-reflected wave traveltimes and the amplitude versus offset (AVO) response of reflectors from the Cardium Conglomerate in the Carrot Creek Field of central Alberta, Canada.

Field data represented by 12 km of 3-component reflection seismic collected over 2 lines and numerous well logs are provided as the data base for the area. Synthetic events that closely represent Cardium reflections based on kinematics were obtained and gave a good idea about the structure velocity of the area. Cardium reflections were studied in terms of AVO using the conventional processing parameters. Further analysis of AVO effects on Cardium boundaries were conducted by considering substantial differences in Poisson's ratio between the Cardium layer and the surrounding media.

All modelling results demonstrate the importance of considering Poisson's ratio in AVO studies. Poisson's ratio has a strong effect on changes in reflection coefficient as a function of the incident angle. With substantial differences of Poisson's ratio across the reflecting interface, polarity reverse may occur depending on the velocity contrast between the two media. In this specific area where the Cardium Conglomerate exists as thin interval, considerable difficulties are experienced in resolving independent formation boundaries. In investigating possible Poisson's ratios for one medium, it is found that the medium boundaries can have the same response for the different cases assumed. Event tuning is also shown to be a result of considering Poisson's ratio.

INTRODUCTION

Numerical modelling is widely used as a useful way to investigate and understand many of the problems in Exploration Seismology. The current study uses numerical modelling, as its tool, to investigate P-SV wave arrival and Amplitude Versus Offset (AVO) on surface seismic data recorded in the Carrot Creek area of central Alberta, Canada.

P-SV wave arrival

P-waves traveling through the subsurface media and reflecting off a boundary produce SV- waves in addition to the P-wave (same type wave) reflections. This indicates that the same source (P-wave source) can be used to record the two-component data; i.e. P-P waves and P-SV waves. The mode-converted wave (P-SV) image acquired by inline horizontal (radial) -component recording provides another seismic image in addition to that obtained from the conventional vertical component.

Wood (1979) showed through amplitude response curves from model data that P-SV raypaths are commonly the largest amplitude converted wave reflections. He claimed that these amplitudes are more dependent on shear velocity contrast than on compressional velocity contrast. Garrota (1987) also considered and confirmed the previous observation by stating that the energy in a P-SV reflection resulting from wave-mode conversion upon

reflection should be much greater than that resulting from conversion upon transmission through an interface above the reflector. He also stated that this P-SV converted wave energy can be an appreciable fraction of the reflected P-wave energy.

Amplitude Versus Offset (AVO)

The seismic reflection amplitude at an elastic boundary is a function of seven parameters, three elastic constants in each medium, the P-wave velocity, the S-wave velocity and density, and the angle of incidence. These elastic constants are functions of mineralogy, lithology and pore fluids. Another important parameter is the change of Poisson's ratio (σ) across the boundary between the target layer and the surrounding (overlying and underlying) media.

One way of analyzing seismic amplitudes is using relative instead of absolute amplitudes. The resulting amplitude behavior can then be properly interpreted in terms of offset changes. Koefoed (1955) demonstrated the variation of reflection coefficients with the angle of incidence in the range between 0° and 30° for considerable difference in Poisson's ratio across the reflecting interface. Ostrander (1984) noticed this variation and used it to detect bright spots in gas sands reflections with non-normal angles of incidence. Chiburis (1984) also gave an example for the importance of Poisson's ratio in detecting fluid-saturated formations.

STUDY AREA

The study area of this project is the Carrot Creek Field of west-central Alberta near Edson, Townships 52 and 53, Ranges 12 and 13, West of Fifth Meridian. In this area, offshore sandbars and ?fluvial conglomerates of the Cardium Formation (Cretaceous) are the exploration targets as they are good oil-producers. The Cardium Conglomerate of the Carrot Creek Field is a poorly sorted chert pebble conglomerate with a sandstone or silty shale matrix (Swagor, 1975). The maximum thickness of the conglomerate is 19 m and it lies at a depth of about 1500 m below the surface. It has a higher P-wave velocity than the encompassing shales of the Colorado group. Wren (1984) showed that the peak corresponding to the Cardium pay in this area is a maximum and most coherent at an intermediate range (660 m - 858 m) of offset.

The field data available in this area contains two (12 km) 3-component reflection seismic lines, CC-SW-01 and CC-SW-02 (Figure 1), and numerous logs recorded in the wells drilled in the area.

STUDY OBJECTIVES

With numerical modelling, a first objective is to obtain synthetic events that closely represent the Cardium reflections (top and bottom interfaces) from a kinematic point of view. This, if achieved, would give us a good idea about the subsurface velocities. A second objective is to consider amplitude versus offset (AVO) on Cardium reflections with conventional processing parameters. This is mainly taking a constant v_p/v_s (i.e. constant Poisson's ratio) as assumed in data processing stream. The following objective is to study the effects of changing Poisson's ratio across the Cardium boundaries and then, study and interpret its consequent AVO observations.

NUMERICAL METHOD AND THEORY

The numerical method used here in this study is based on raytracing theory. The Sierra Geophysics modelling was used to generate synthetic shot gathers for a specified geologic model and source-receiver array. The program uses asymptotic ray theory to

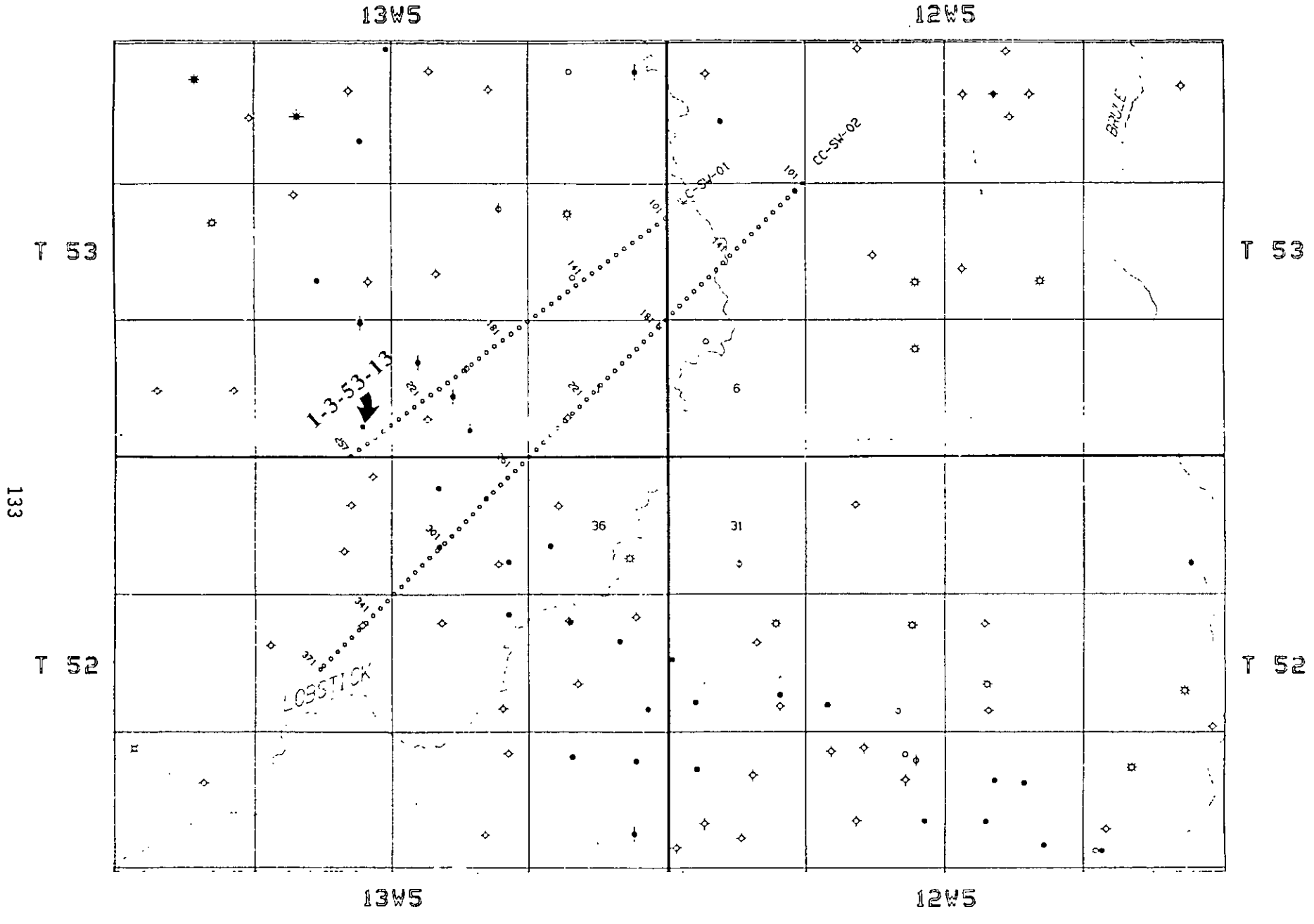

Figure 1: Shot point map showing the two seismic lines, CC-SW-01 and 02. Also, well location 1-3-53-13 is shown.

obtain seismic amplitudes, modelling offset dependent reflection/transmission losses and geometric attenuation. A P-wave source is used to send energy from each shot surface position while vertical and inline horizontal geophones are used to receive the reflected energy coming back up to the surface.

The P-wave velocities v_p and the Poisson's ratio σ for each layer are the known values. The S-wave velocities are found from

$$v_S = v_p \left[\frac{1 - 2\sigma}{2(1 - \sigma)}\right]^{\frac{1}{2}}$$

The density ρ of each layer is obtained from Gardner et. al., (1974);

$$\rho = 0.23 \left[V_P\right]^{\frac{1}{4}}$$

In raytracing, the raypath satisfy Snell's Law;

$$\frac{\sin i}{v_i} = \frac{\sin o}{v_o}$$

where, i and o are the incoming and outgoing angles between the ray and the normal. v_i and v_o are the incident and outgoing wave velocities. Snell's law is valid for both reflection and transmission with the appropriate velocities.

The ray traveltime is given by

$$t = \sum_i \left\langle \frac{d_i}{v_i} \right\rangle + \vec{P} \cdot \delta\vec{x}$$

where d_i and v_i are the distance and velocity of the i^{th} leg of the ray respectively, and $\vec{P}$ is the ray parameter vector at the receiver while $\delta\vec{x}$ is the vector describing the difference between the captured ray emergence point and the receiver point . This says that the term $\vec{P} \cdot \delta\vec{x}$ is a correction term added to the equation to interpolate for the ray not exactly captured on the receiver point.

In amplitude calculations, anelastic attenuation is not allowed. Hence, the two other factors considered are the transmission-reflection energy loss and the geometric spreading. Transmission-reflection effects occur at velocity and density variations where plane wave transmission and reflection coefficients are computed (Aki and Richards, 1980) at each interface. The geometric spreading can be explained as the decrease of amplitude with distance. The method used to account for the geometric spreading is the **WKBJ** approximation.

SYNTHETIC MODELS

The first step in raytracing is to propose a geologic model for the area of study. Performing a blocking procedure on a sonic log that was conducted in the well 1-3-53-13 very near to the seismic line CC-SW-01 in the Carrot Creek Field (Figure 1) introduced a flat multi-layer geologic model with a P-wave velocity determined for every layer in the model. The velocities picked were then reduced by 10% to compensate for the high frequency (greater velocity) sonic acquisition (Yilmaz, 1987). Figure 2 shows the proposed geologic model in this area with the corresponding P-wave velocities estimated.

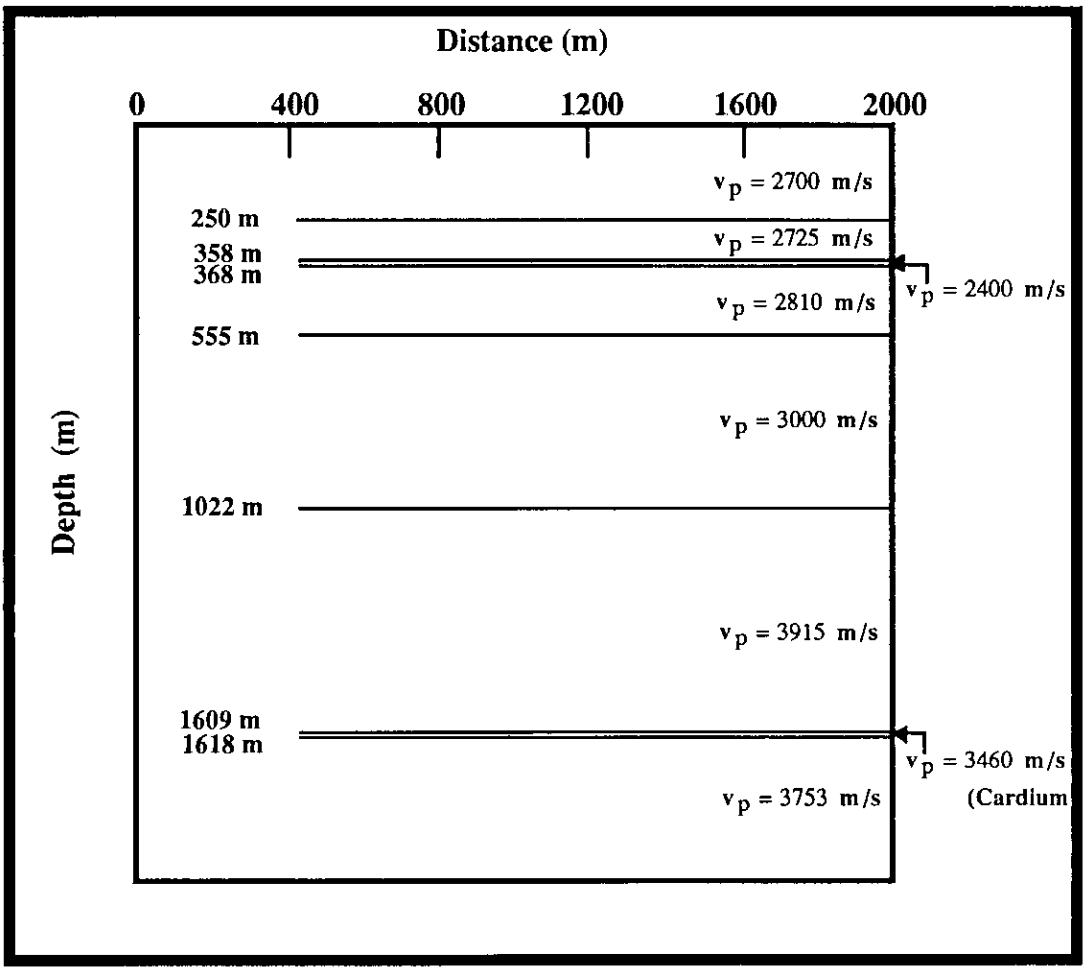

Figure 2: Assumed geologic model in Carrot Creek area with the estimated corresponding P-wave velocities

For the array geometry, five shots are considered here. The shots are arranged from 1 to 5 starting with no. 1 as an end-on shot (with trace 1 ahead). There are 80 receivers to record the signal with a 30 m group interval. The gap between the shot and the near receiver is 6 group intervals (180 m). The geometry of the shot move-up is that no. 1 is an end-on shot, shot 2 moves up by 10 traces so it would have 10 traces behind and 70 traces ahead. And so on with a 10-trace increment until shot no. 5 is a symmetrical split-spread (with 40 traces behind and 40 ahead).

As an initial effort to study AVO on Cardium reflections, The ratio of the P-wave velocity to the S-wave velocity, v_p/v_s, is taken to be 1.92 (σ = .31) for the entire model as it was assumed in conventional processing parameters. To go further in the analysis of AVO, The Cardium along with its surrounding (overlying and underlying) layers are substituted in separate models with the same P-wave velocity but with different Poisson's ratio (P. R.) in order to change the S-wave velocity which, in turn, might affect the amplitude of a reflection at certain angle of incidence. In these models, an ideal shale P. R. of .36 at a moderate depth (Birch, 1942) is given and kept the same for the overlying and underlying shale layers. For the Cardium layer itself, a range of .15 to .35 with .05 increment was used for the Cardium P. R. to see the reflection response in each case with

the surrounding media. Table 1 gives the details of the computed values for all model cases. The following points have to be noted however;

- The density ρ and the P-wave velocity v_p are always the same for all models
- The case **a. Constant P. R.** is performed with conventional processing parameters ($\sigma = .31$)
- The case **b. Variable P. R.** had the variation only in the Cardium P. R. while P. R. is kept the same (.36) for the overlying and underlying layers (this is shown by the similar v_s and v_p/v_s in every case)

RESULTS AND DISCUSSION

a. Constant Poisson's Ratio:

For the first set of models where we followed the conventional processing parameter of applying constant Poisson's ratio of .31 through the entire geologic model, separate raytracing processes were run to obtain synthetic events for the both the top and bottom of the Cardium in the case of P-P wave arrivals on the vertical channel (Figure 3). Note that all the records displayed in this study were plotted with the actual computed amplitudes. No scaling of any type was applied on this data. According to the impedance contrast between the layers bounded by these two interfaces, we see a positive-polarity event (Figure 3 (a)) for the top interface (between Cardium and its overlying layer) and a negative-polarity event (Figure 3 (b)) for the bottom interface (between Cardium and its underlying layer). In terms of amplitude variation, an amplitude decrease can be seen in both Figures 3 (a), (b) as the angle of incident (offset) increases. This is the quite known behavior of AVO for constant Poisson's ratio (Muskat and Meres, 1940). The next step in the modelling procedure considered here is that the two separate events for the Cardium are merged together (while they are in the spike seismogram stage) to produce a single event. Figure 4 shows the resultant record where Figure 4 (a) demonstrates the top and bottom of Cardium in shot 1. As seen in this figure, there is no separation between the upper and lower Cardium events. This is due to the Conglomerate thinning in this area, resulting in the very close-spaced events for the top and bottom interfaces. Shots 2-5 are plotted in Figure 4 (b) where a trace for every 3 traces was plotted to represent the changes in traveltime and amplitude for each shot. This figure exhibits minor AVO changes with offset (shot 2).

Now, for P-SV wave arrivals on the radial channel, and again, considering the constant Poisson's ratio case ($\sigma = .31$), Figures 5 and 6 follow the same processes were performed on Figures 3 and 4 respectively. Similar results for event polarity can be seen on Figure 6 (a) and (b). However, the observation here is that the P-SV (radial component) for the Cardium top (Figure 5 (a)) has a higher level of energy than that of the the P-P (vertical component) for the same interface. The amplitude trend of this P-SV arrival is that there is an increase in amplitude with increasing offset until it reaches maximum, maintaining these high amplitude values for long offset range before it starts to decrease with larger offset to minimum at trace 80. The previous observation is confirmed when we look at the merged record for the Cardium top and bottom interfaces (Figure 6(a)). For shots 2-5, the P-SV top and bottom record (Figure 6 (b)) agrees with the theoretical knowledge which states that a polarity change in the center of a split spread shot gather occurs for the P-SV reflection.

	Overlying layer (1)		Cardium (2)		Underlying layer (3)
ρ (gm/cc)	2.37		2.45		2.42
v_p (m/s)	3460		3915		3753
		$v_{p_1}/v_{p_2} = .88$		$v_{p_2}/v_{p_3} = 1.04$	

a. Constant P. R.
($\sigma = .31$)

v_s (m/s)	1803		2040		1955
v_p/v_s	1.92		1.92		1.92
		$v_{s_1}/v_{s_2} = .88$		$v_{s_2}/v_{s_3} = 1.04$	

b. Variable P. R.
(ONLY for Cardium)

1. $\sigma = .15$

v_s (m/s)	1618		2512		1755
v_p/v_s	2.14		1.56		2.14
		$v_{s_1}/v_{s_2} = .64$		$v_{s_2}/v_{s_3} = 1.43$	

2. $\sigma = .20$

v_s (m/s)	1618		2397		1755
v_p/v_s	2.14		1.63		2.14
		$v_{s_1}/v_{s_2} = .68$		$v_{s_2}/v_{s_3} = 1.37$	

3. $\sigma = .25$

v_s (m/s)	1618		2260		1755
v_p/v_s	2.14		1.73		2.14
		$v_{s_1}/v_{s_2} = .72$		$v_{s_2}/v_{s_3} = 1.29$	

4. $\sigma = .30$

v_s (m/s)	1618		2093		1755
v_p/v_s	2.14		1.87		2.14
		$v_{s_1}/v_{s_2} = .77$		$v_{s_2}/v_{s_3} = 1.19$	

5. $\sigma = .35$

v_s (m/s)	1618		1881		1755
v_p/v_s	2.14		2.08		2.14
		$v_{s_1}/v_{s_2} = .86$		$v_{s_2}/v_{s_3} = 1.07$	

Table 1: Modelling parameters and their order in the models considered

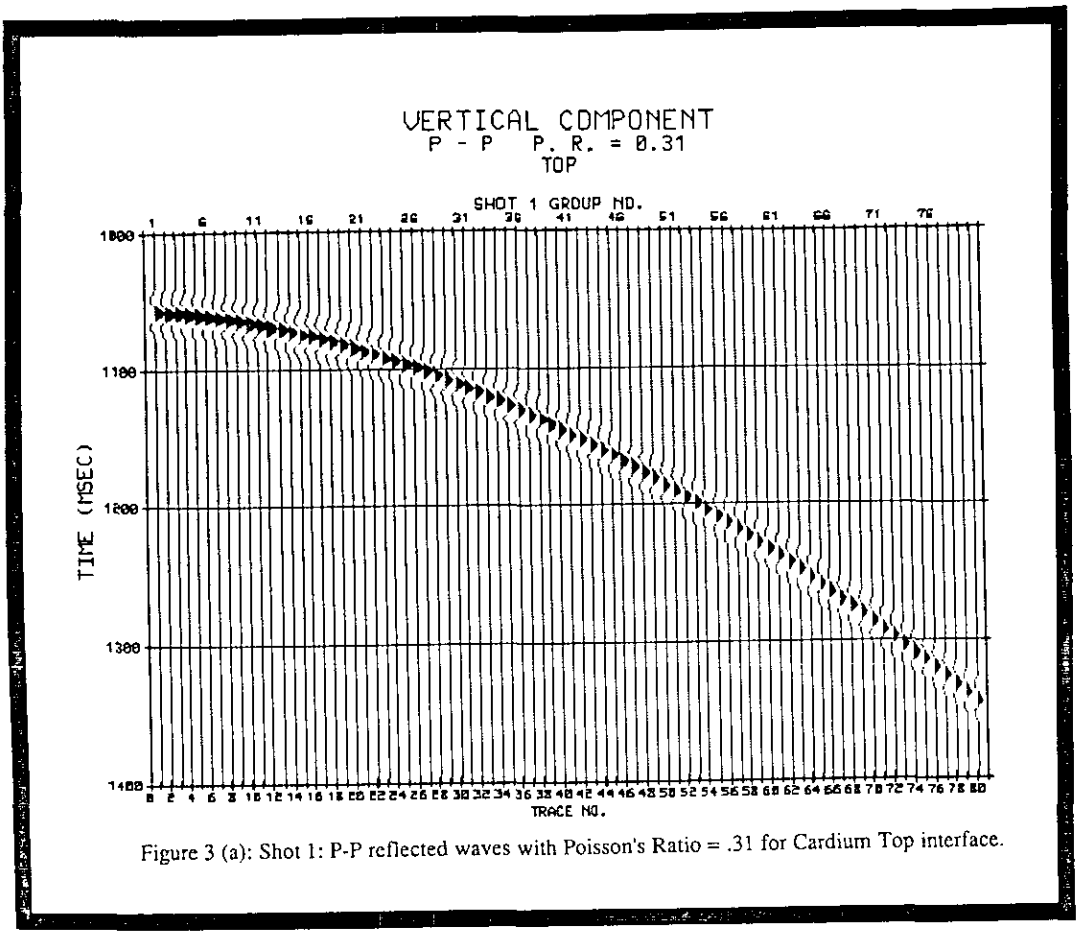

Figure 3 (a): Shot 1: P-P reflected waves with Poisson's Ratio = .31 for Cardium Top interface.

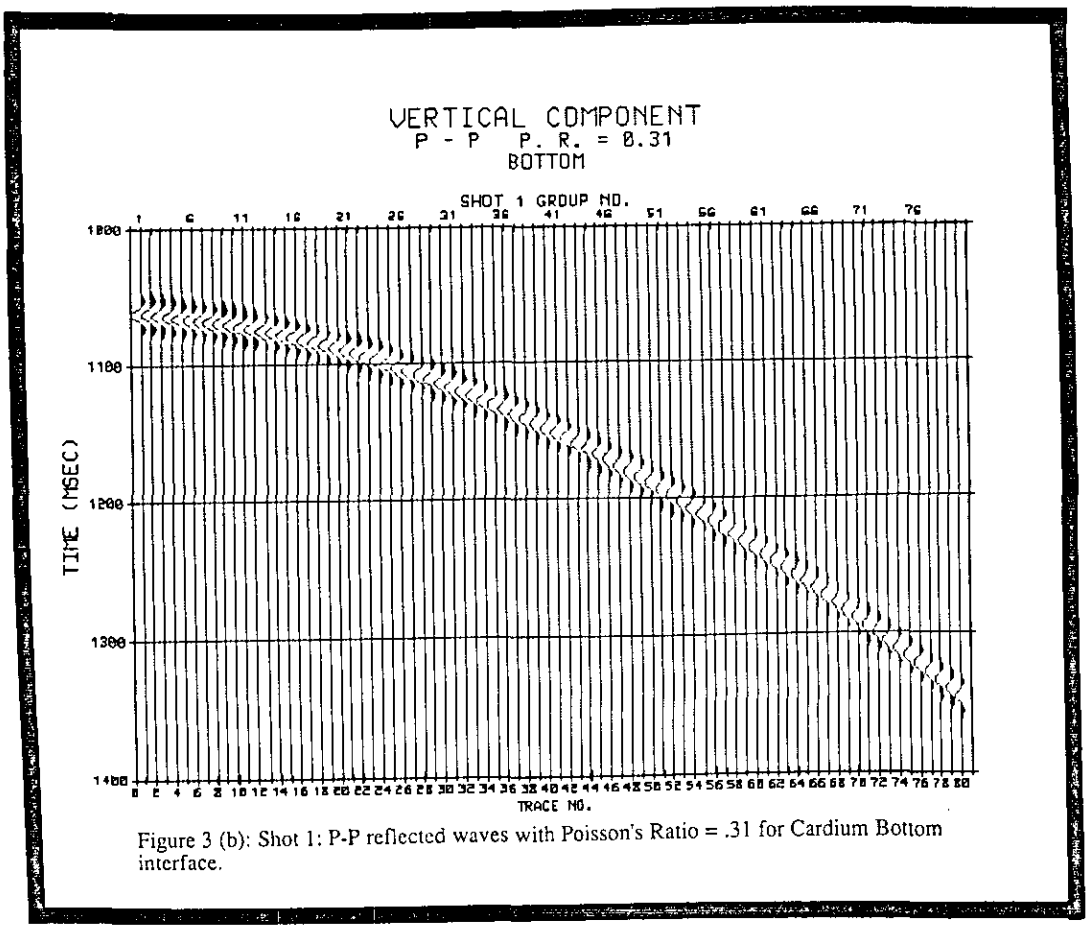

Figure 3 (b): Shot 1: P-P reflected waves with Poisson's Ratio = .31 for Cardium Bottom interface.

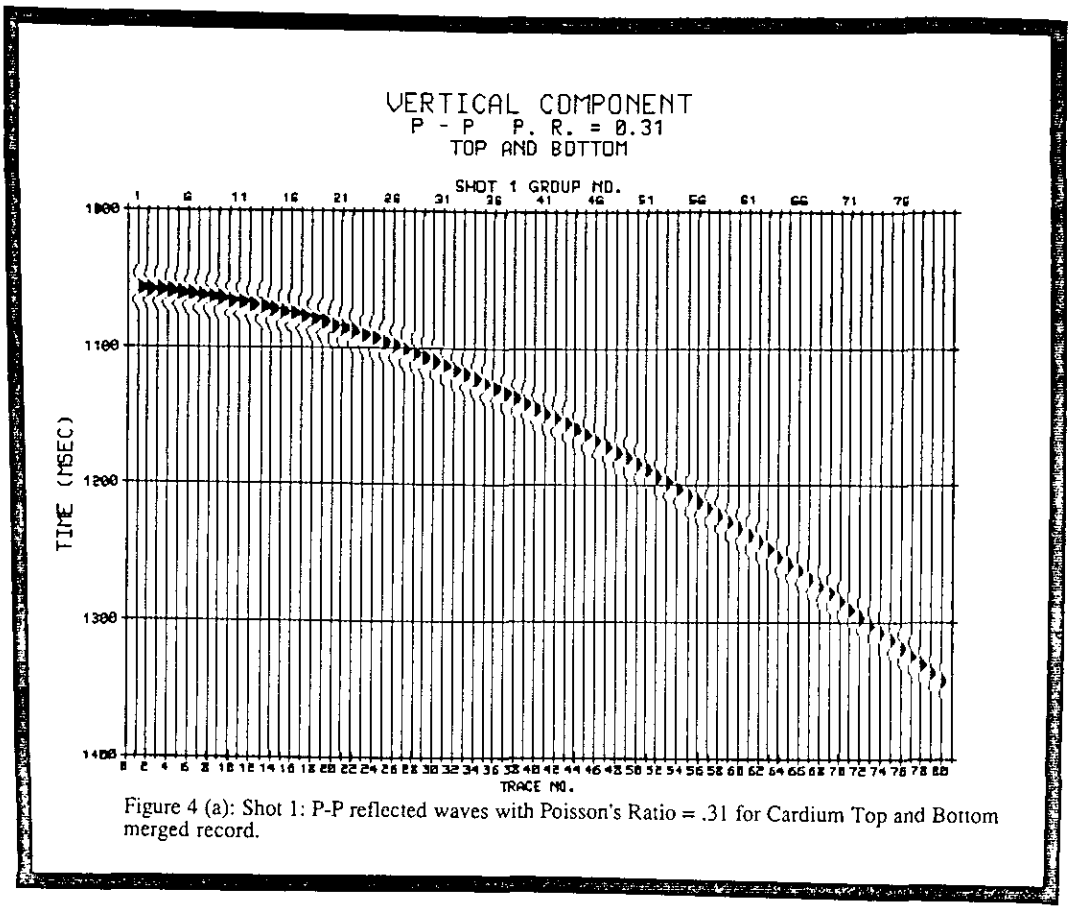

Figure 4 (a): Shot 1: P-P reflected waves with Poisson's Ratio = .31 for Cardium Top and Bottom merged record.

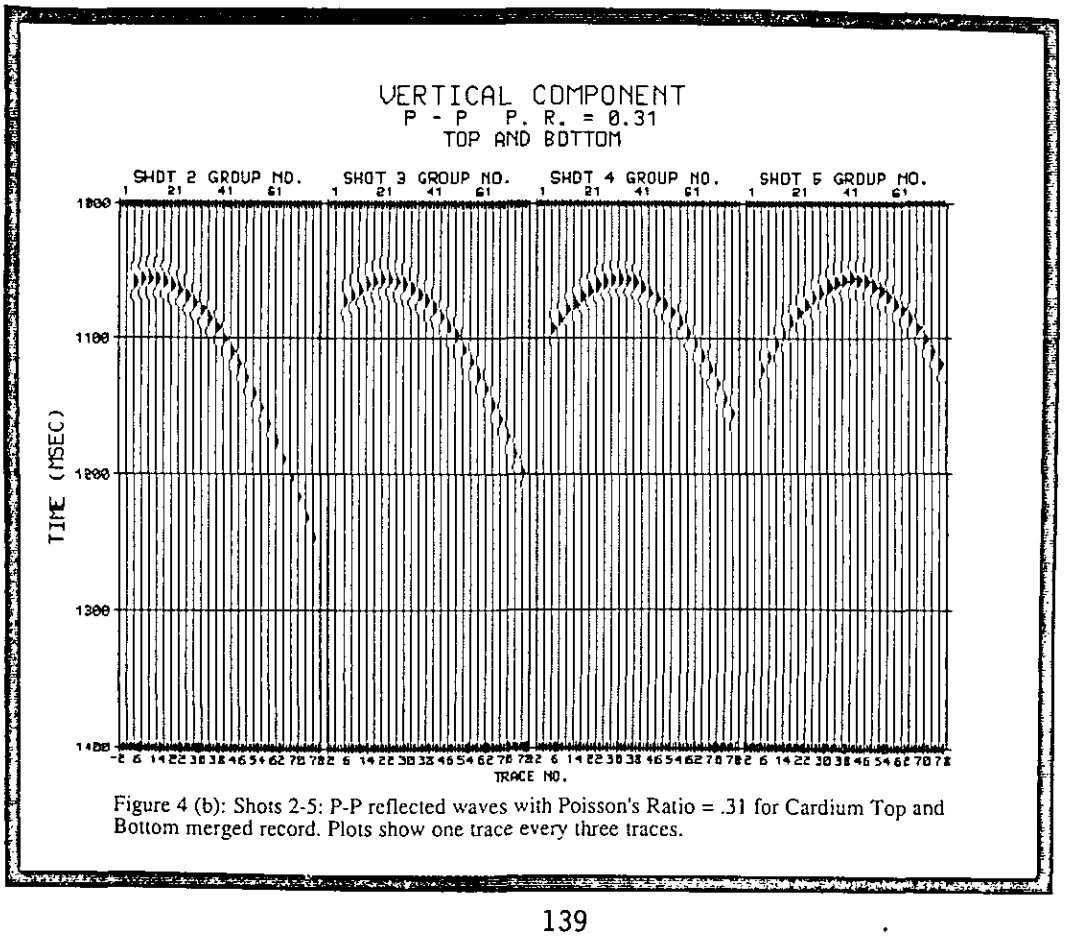

Figure 4 (b): Shots 2-5: P-P reflected waves with Poisson's Ratio = .31 for Cardium Top and Bottom merged record. Plots show one trace every three traces.

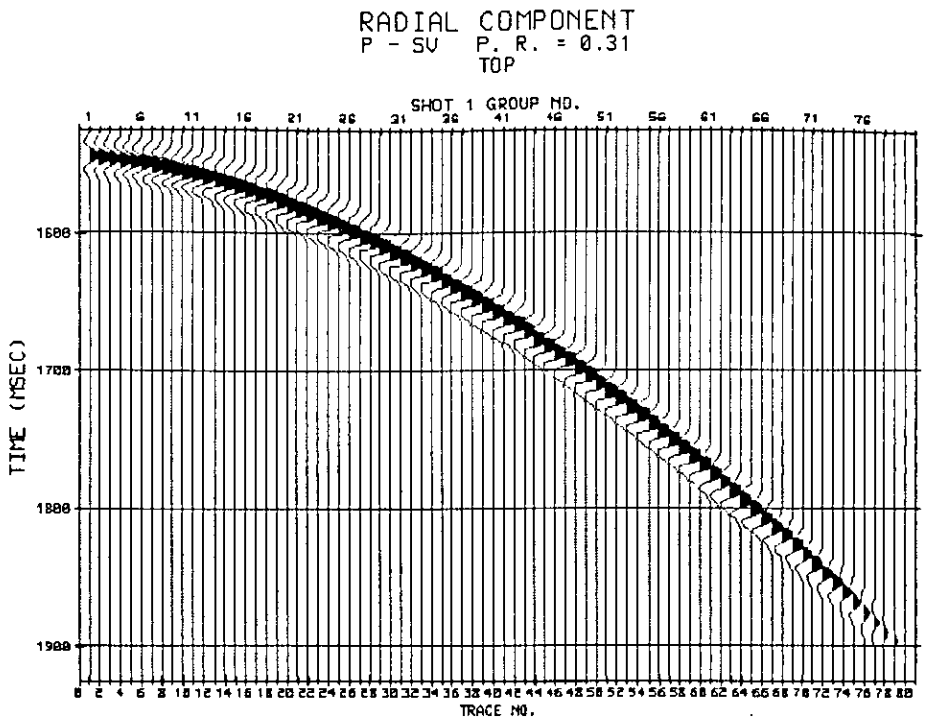

Figure 5 (a): Shot 1: P-SV reflected waves with Poisson's Ratio = .31 for Cardium Top interface.

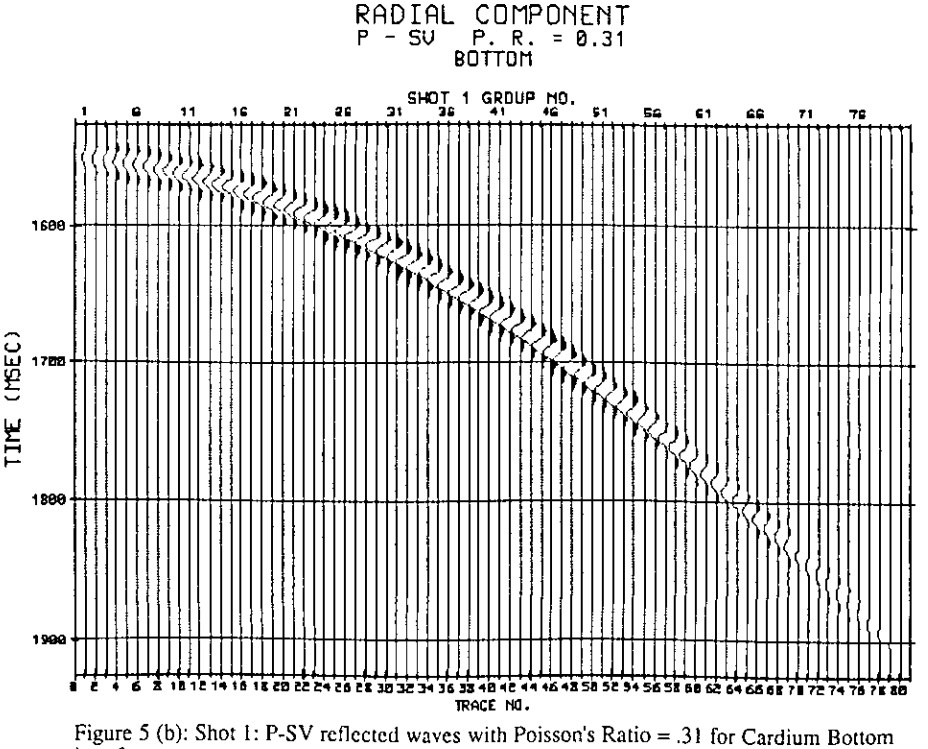

Figure 5 (b): Shot 1: P-SV reflected waves with Poisson's Ratio = .31 for Cardium Bottom interface.

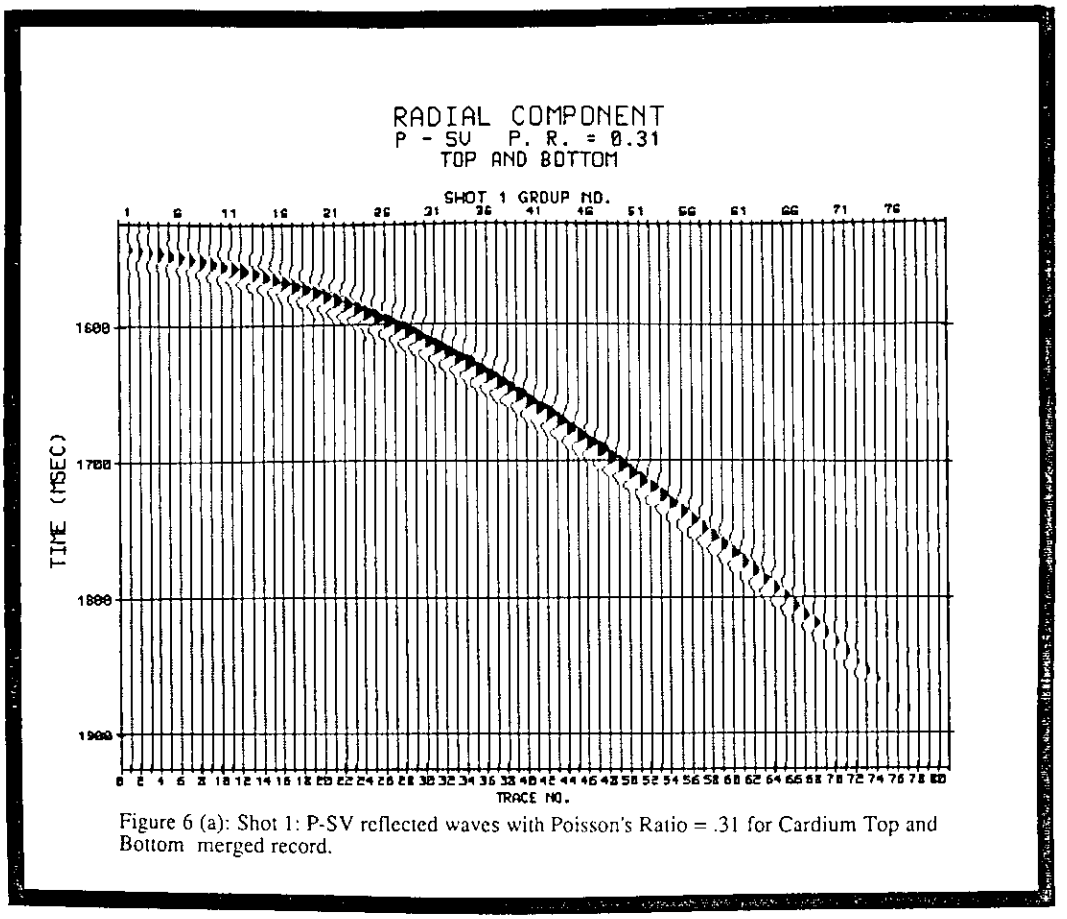

Figure 6 (a): Shot 1: P-SV reflected waves with Poisson's Ratio = .31 for Cardium Top and Bottom merged record.

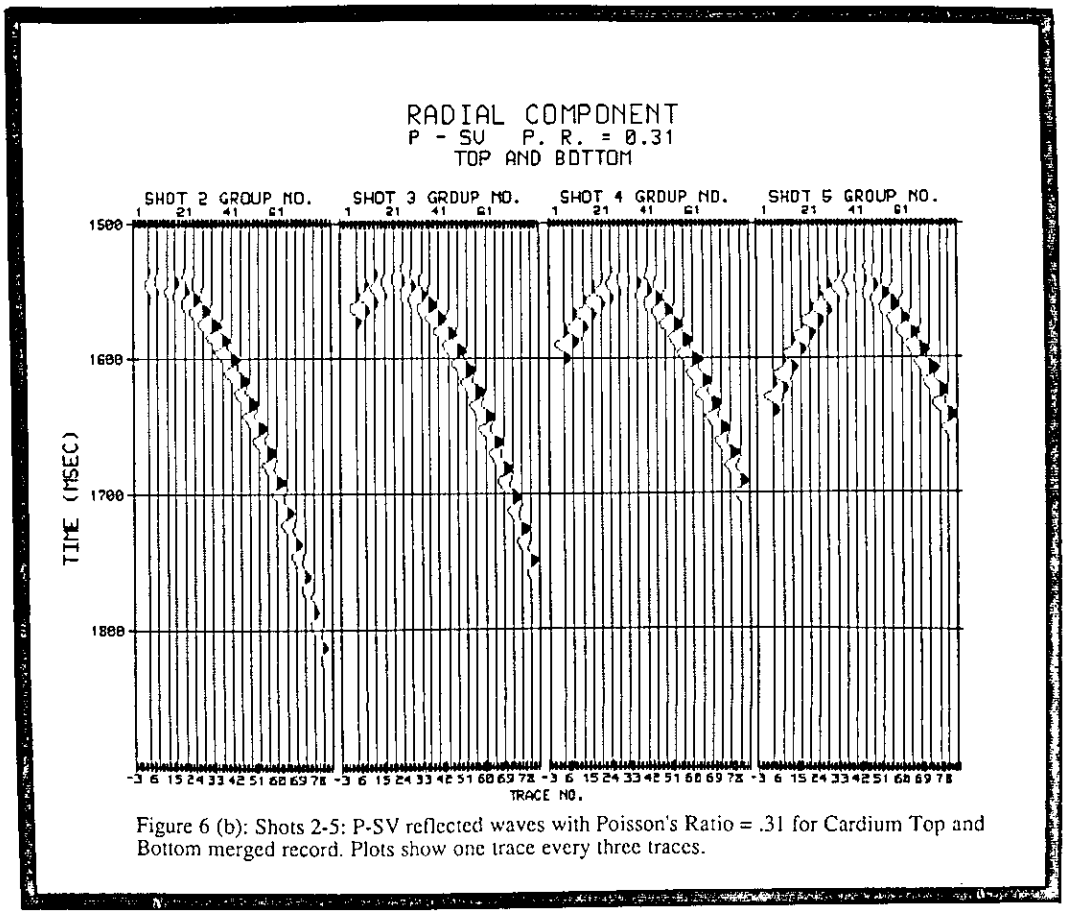

Figure 6 (b): Shots 2-5: P-SV reflected waves with Poisson's Ratio = .31 for Cardium Top and Bottom merged record. Plots show one trace every three traces.

b. Variable Poisson's Ratio:

Considering the further analysis in AVO studies for the effects of Poisson's ratio differences across the interface between the Cardium and its overlying/underlying layer, we start looking at item b in table 1 for the different cases of Poisson's ratio values.

The first Poisson's ratio (σ) is .15 and we again look at P-P waves first. Remember that the surrounding layers from now on have $\sigma = .36$ as mentioned in the synthetic model section. So, for the top interface (Figure 7 (a)), we see that the difference in σ across the interface really affects the amplitude as a function of incident angle. The amplitudes get smaller (in magnitude) until they would be close to zero then they reverse the sign and start to build up in magnitude again as offset increases (Figure 7 (a), (b)). We would expand this interesting feature (polarity reverse) in later analysis on the different cases of σ. With the help of a reflection coefficient and phase computation program [courtesy E. Krebes] of the University of Calgary, we note that this change in polarity occurs on trace $\cong$ 39 with angle of incidence $\theta \cong 26^\circ$ (Figure 7 (a)) for the Cardium top while occurred on trace $\cong$ 15 with $\theta \cong 14^\circ$ (Figure 7 (b)) for the Cardium bottom. What we learn from this observation is that for a certain σ, polarity change occurs at Cardium reflections but with an incident angle θ on bottom boundary that is less than that on top boundary. In looking at the P-SV arrival, we see that the top boundary (Figure 8 (a)) exhibits no polarity change even though the difference in σ is very significant. But, when we see that the bottom reflector has a polarity change at trace $\cong$ 63 with $\theta \cong 57^\circ$ and use the previous result from the P-P case about the occurrence of polarity change on the top at a greater θ (nearly twice as much) than that on the bottom, then we can see why polarity does not occur on the top boundary for P-SV case. Figure 9 supports the author's claim that the P-SV (Figure 9 (b)) on the radial channel has higher energy than that of the P-P (Figure 9 (a)) on the vertical channel.

The Cardium top boundary of the rest of σ values does not show any more significance than what we have seen on the corresponding one when $\sigma = .15$ (Figure 8 (a)). What we are interested in investigating for the the rest of these σ values belong to the following observations.

Firstly, considering the P-SV cases when $\sigma = .25$ and .30 for the Cardium bottom (Figure 10 (a) and (b)), we observe that there is a "move up" of the polarity change with the increase of Poisson's ratio (σ) which causes the S-wave velocity to decrease for the Cardium. From Table 1 , we can see that the increase in σ leads the shear velocity contrast between the Cardium and the underlying layer to get smaller. The effect of this decrease in the velocity contrast is the direct reason for the occurrence of polarity change at a further offset as we increase σ. By reviewing the computation with the available program, it was found that for $\sigma = .25$ (Figure 10 (a)), the incident angle at which polarity changes is $\theta \cong 63^\circ$ and for $\sigma = .30$ (Figure 10 (b)), θ was found to be $\cong 67^\circ$.

Secondly, a comparison among Figures 11 (a), (b) and (c) which are the events of P-SV arrival for the top and bottom record when $\sigma = .15$, .20 and .25, respectively, show that the three records are almost identical in their traveltime and amplitude information. This indicates that if we are to perform the inverse problem for the three records, the result would not be a unique solution for the value of σ. What can be understood at this time is that even for different Poisson's ratios in one medium, the interface bounding this medium can give similar signature.

Thirdly, when $\sigma = .30$, the top and bottom record (Figure 11 (d)) has a different event from the one in the previous three. Observing the top and the bottom of this record separately for this value of σ, it was found that when the two events merged, they constructively interfered and gave the resultant high amplitude record (Figure 11 (d)). This is what is referred to event tuning.

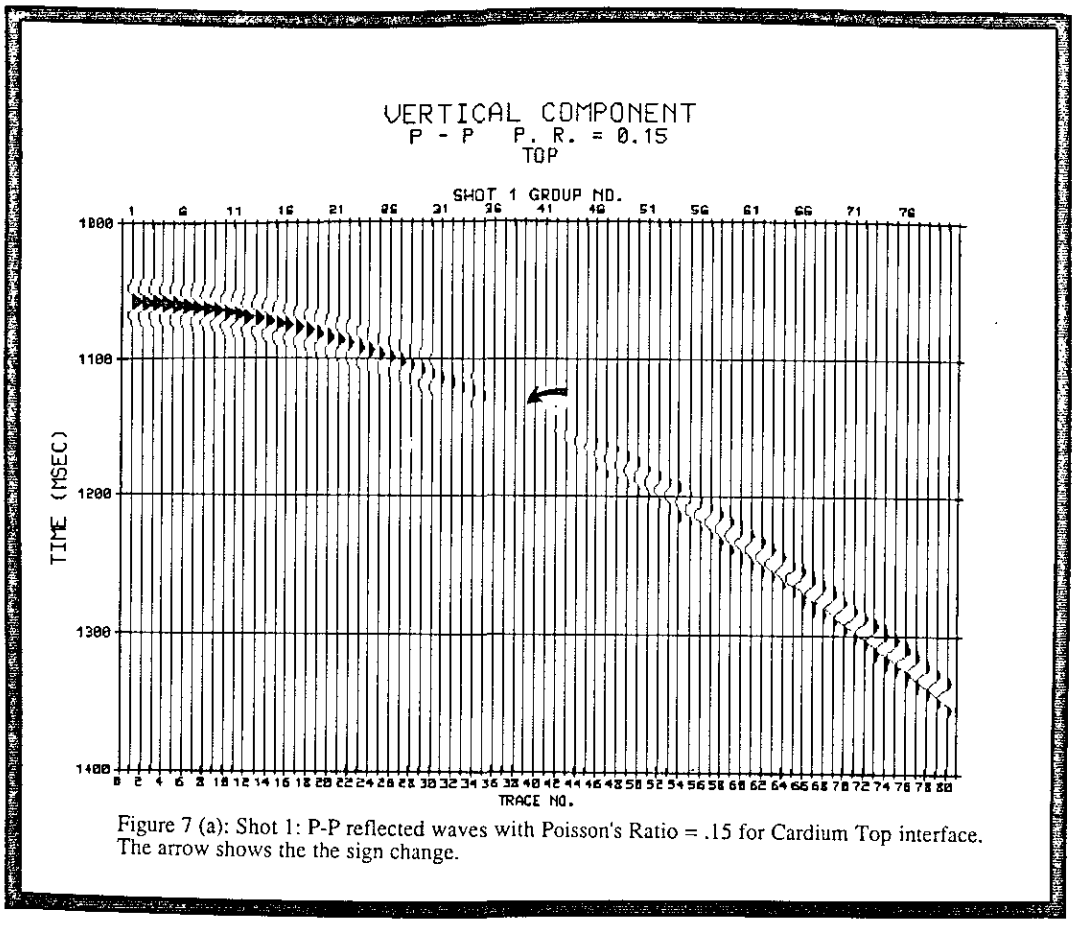

Figure 7 (a): Shot 1: P-P reflected waves with Poisson's Ratio = .15 for Cardium Top interface. The arrow shows the the sign change.

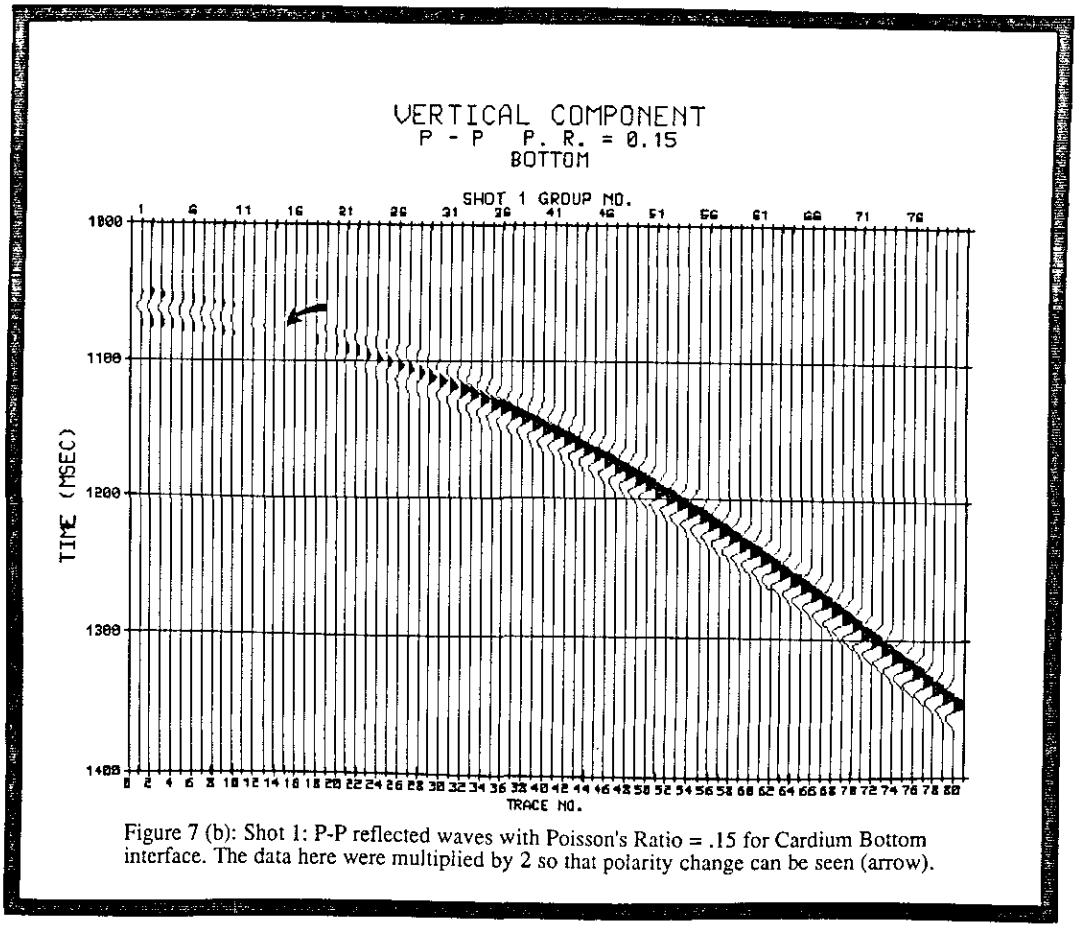

Figure 7 (b): Shot 1: P-P reflected waves with Poisson's Ratio = .15 for Cardium Bottom interface. The data here were multiplied by 2 so that polarity change can be seen (arrow).

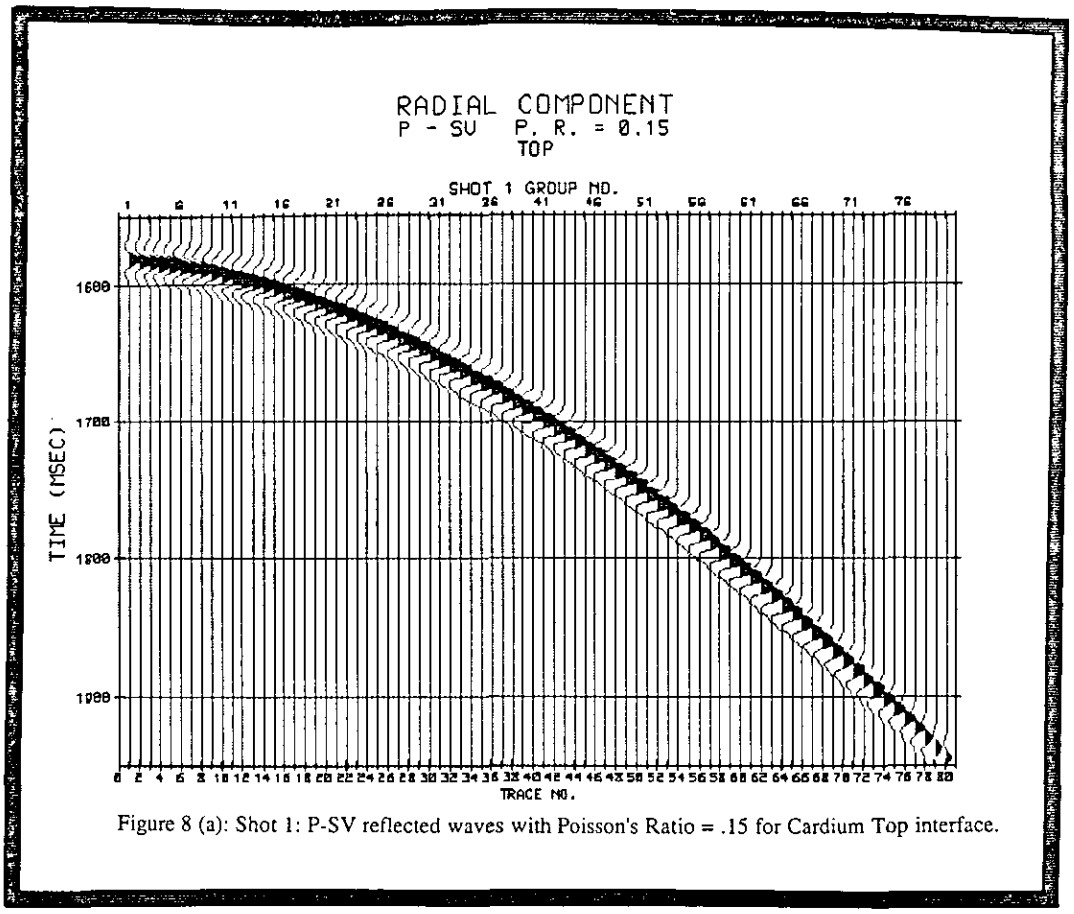

Figure 8 (a): Shot 1: P-SV reflected waves with Poisson's Ratio = .15 for Cardium Top interface.

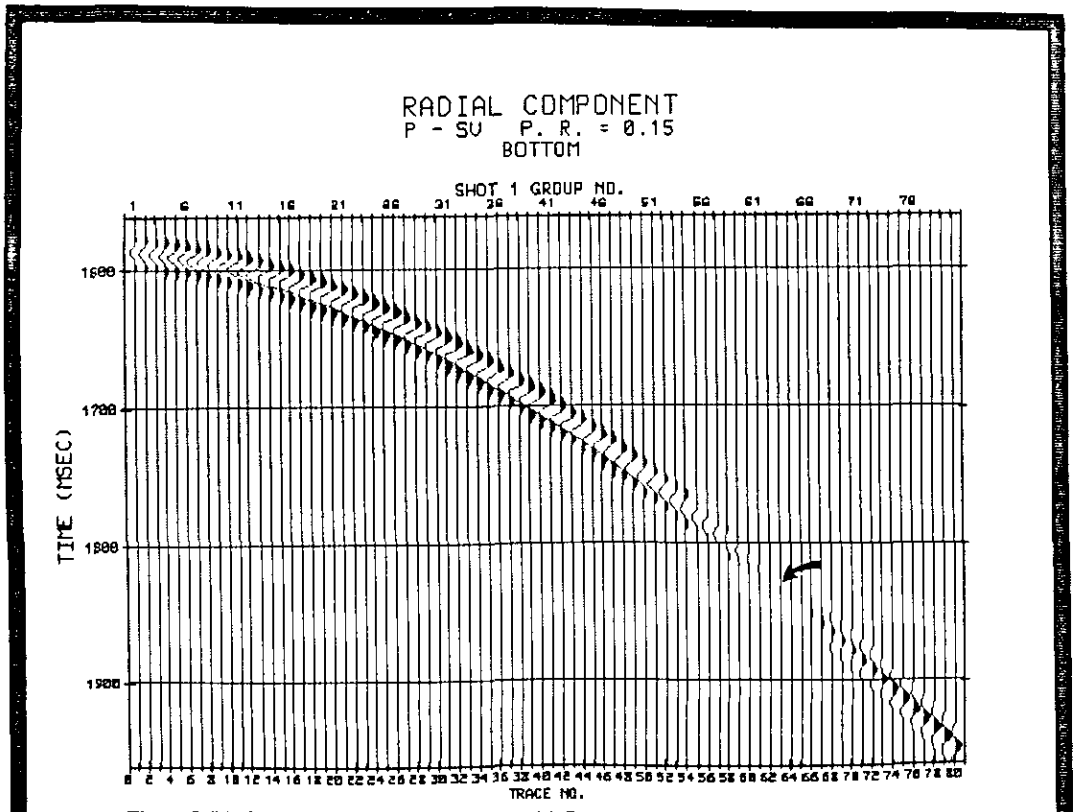

Figure 8 (b): Shot 1: P-SV reflected waves with Poisson's Ratio = .15 for Cardium Bottom interface. The arrow shows the sign change.

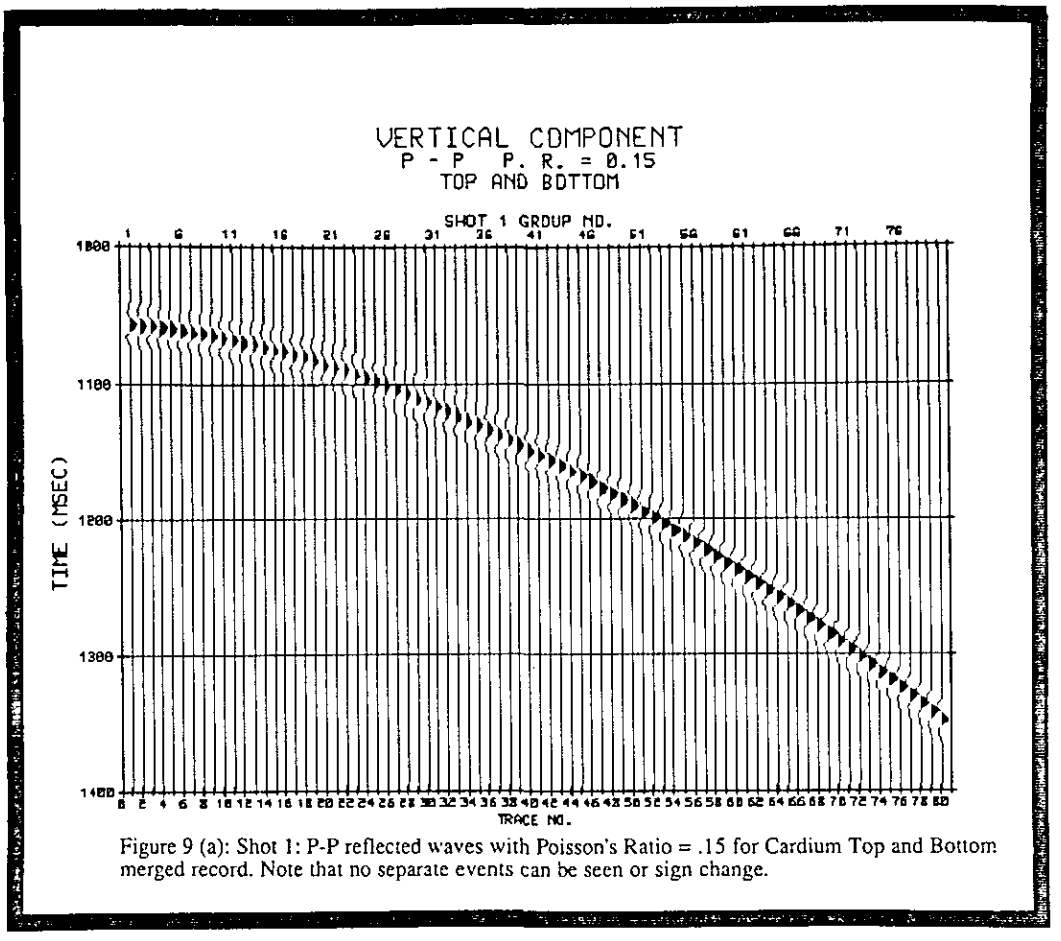

Figure 9 (a): Shot 1: P-P reflected waves with Poisson's Ratio = .15 for Cardium Top and Bottom merged record. Note that no separate events can be seen or sign change.

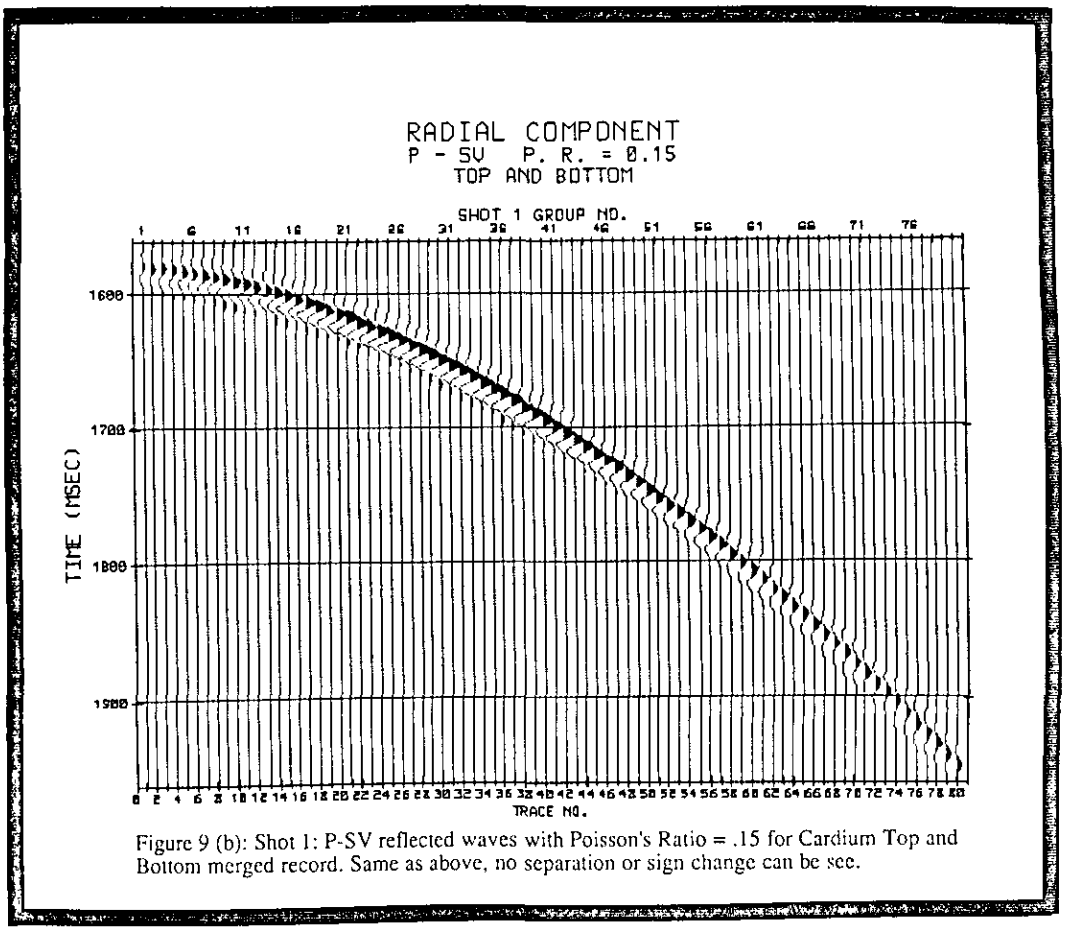

Figure 9 (b): Shot 1: P-SV reflected waves with Poisson's Ratio = .15 for Cardium Top and Bottom merged record. Same as above, no separation or sign change can be see.

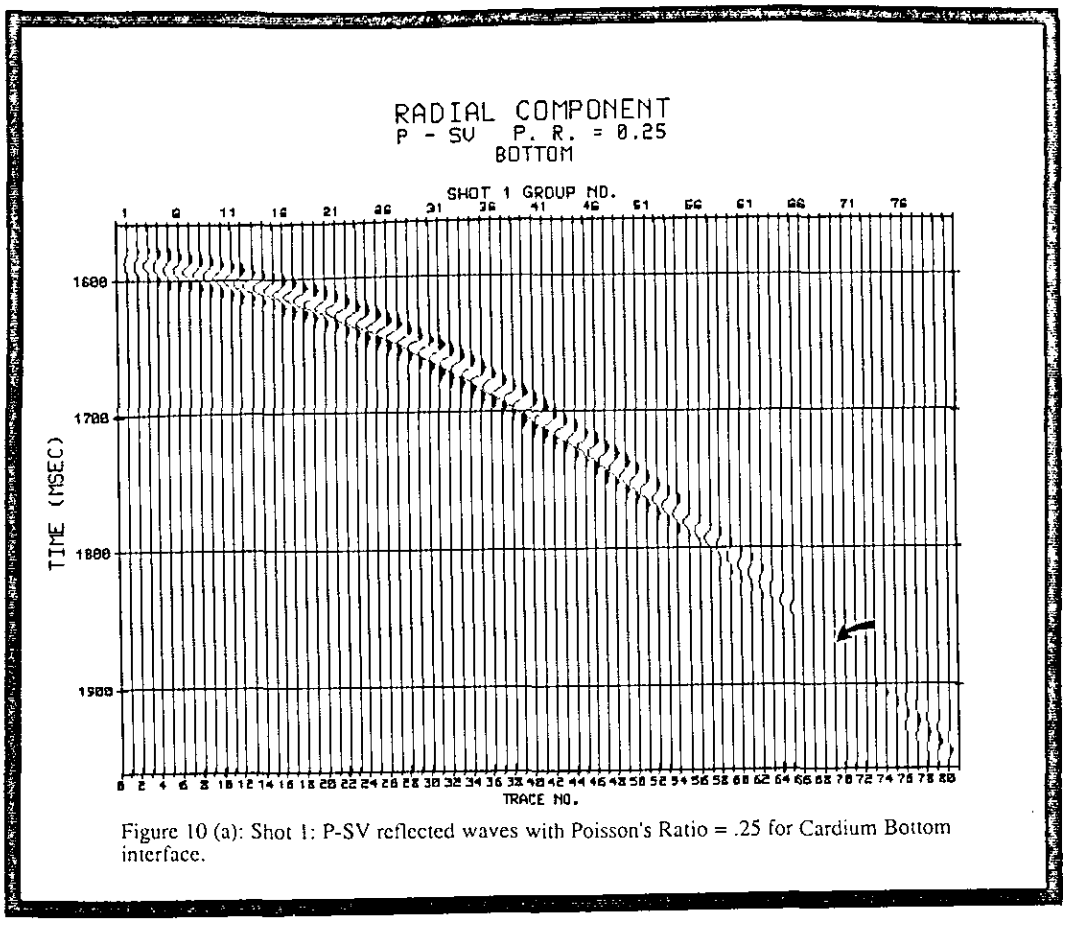

Figure 10 (a): Shot 1: P-SV reflected waves with Poisson's Ratio = .25 for Cardium Bottom interface.

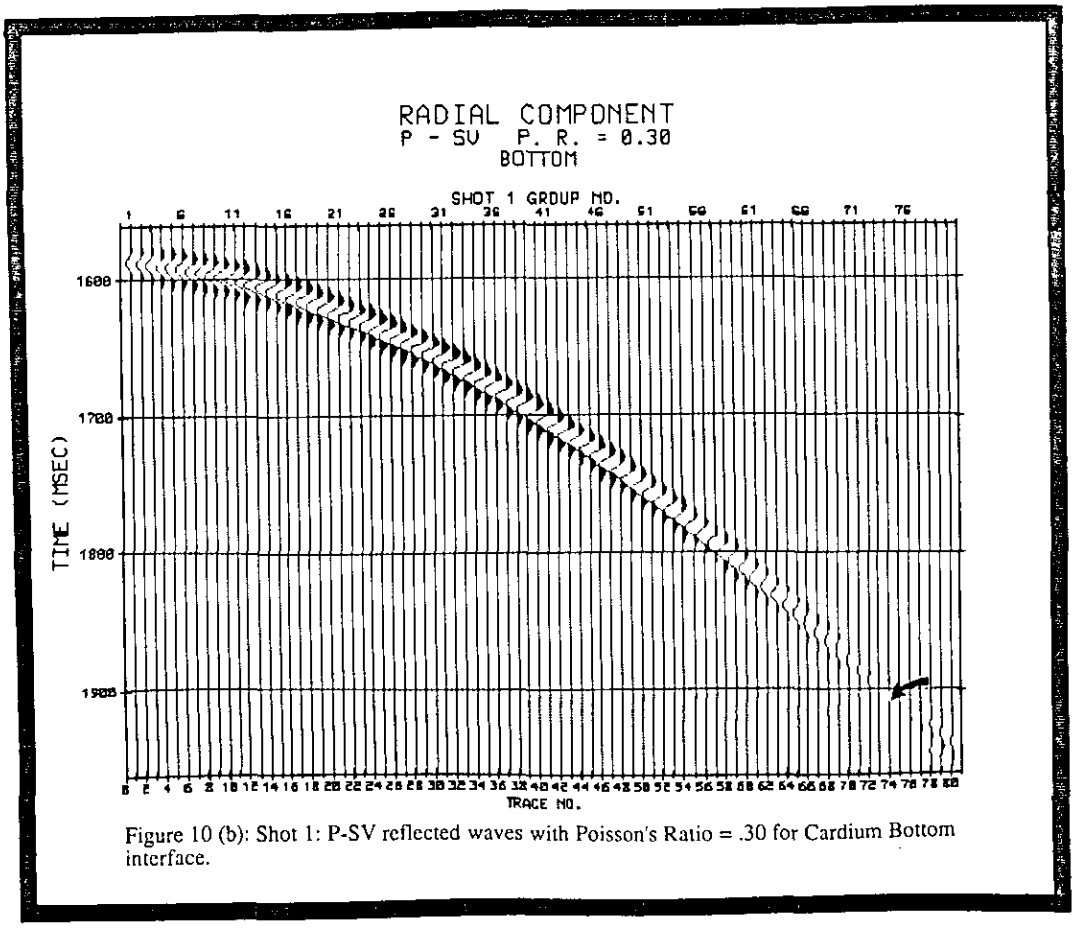

Figure 10 (b): Shot 1: P-SV reflected waves with Poisson's Ratio = .30 for Cardium Bottom interface.

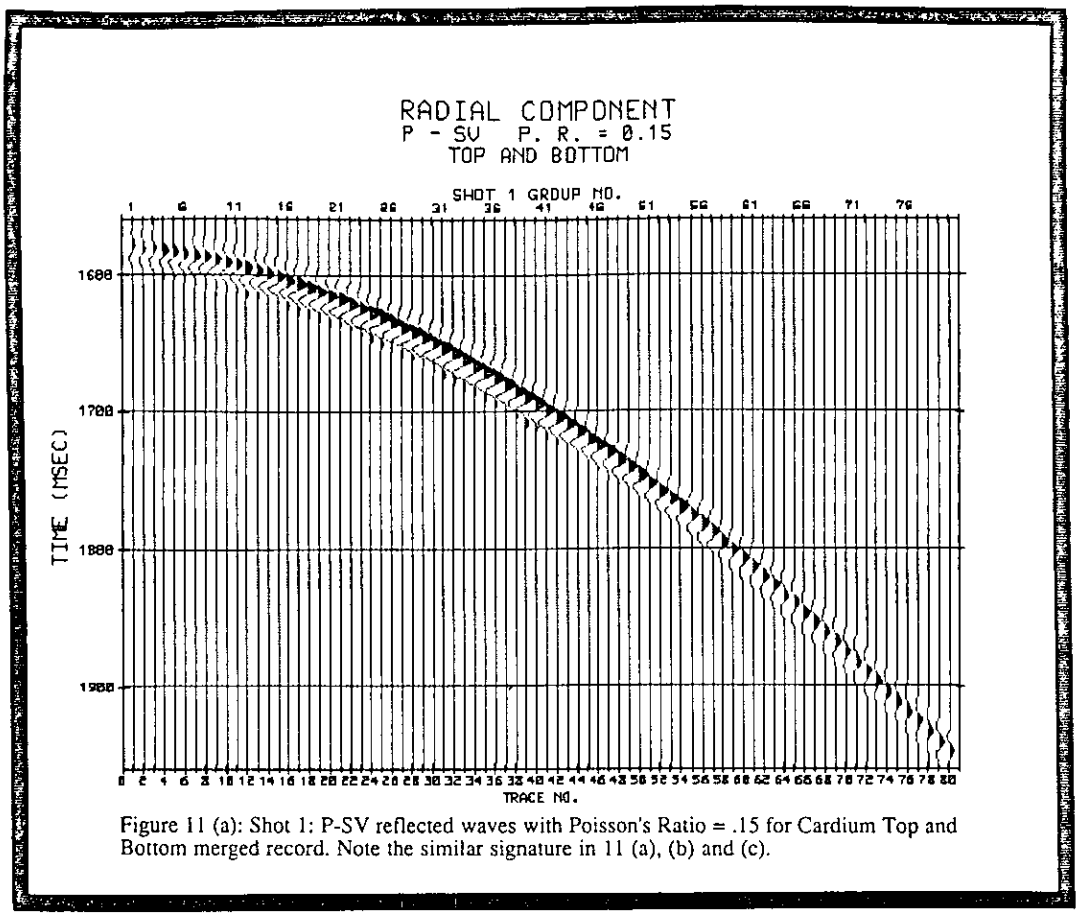

Figure 11 (a): Shot 1: P-SV reflected waves with Poisson's Ratio = .15 for Cardium Top and Bottom merged record. Note the similar signature in 11 (a), (b) and (c).

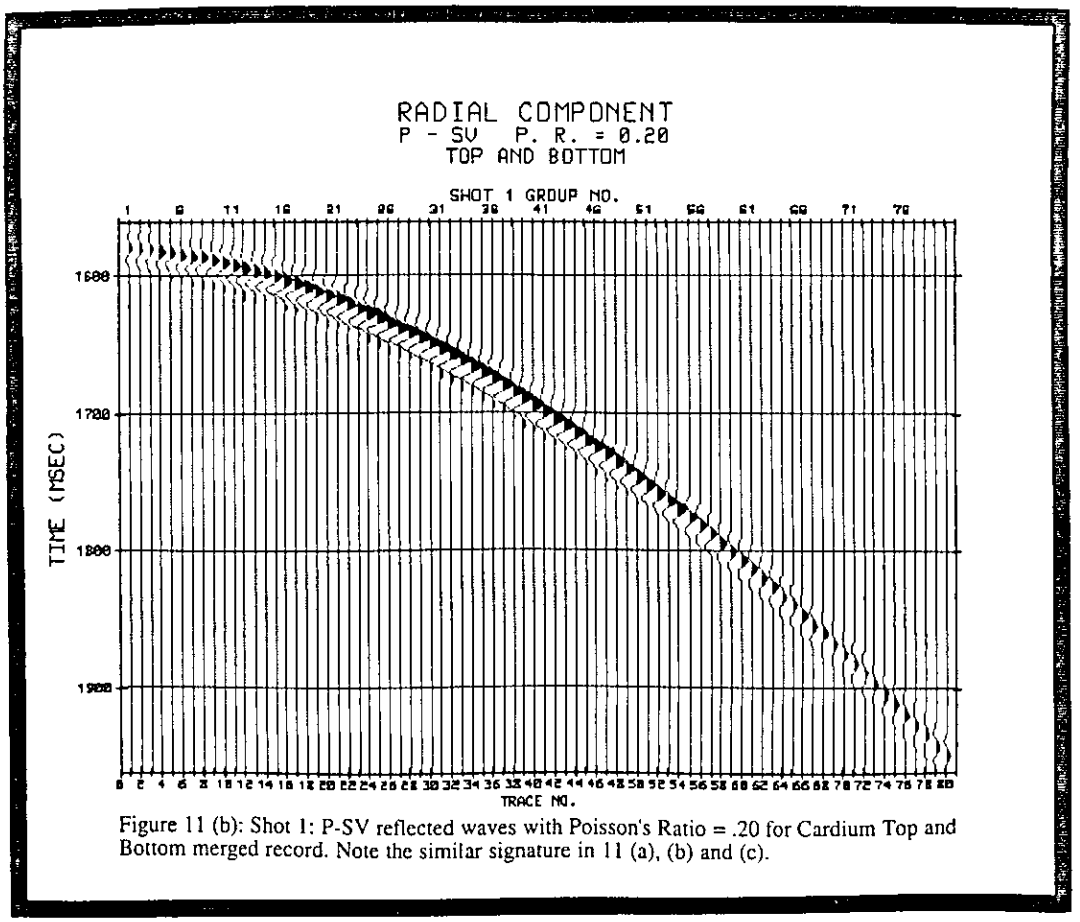

Figure 11 (b): Shot 1: P-SV reflected waves with Poisson's Ratio = .20 for Cardium Top and Bottom merged record. Note the similar signature in 11 (a), (b) and (c).

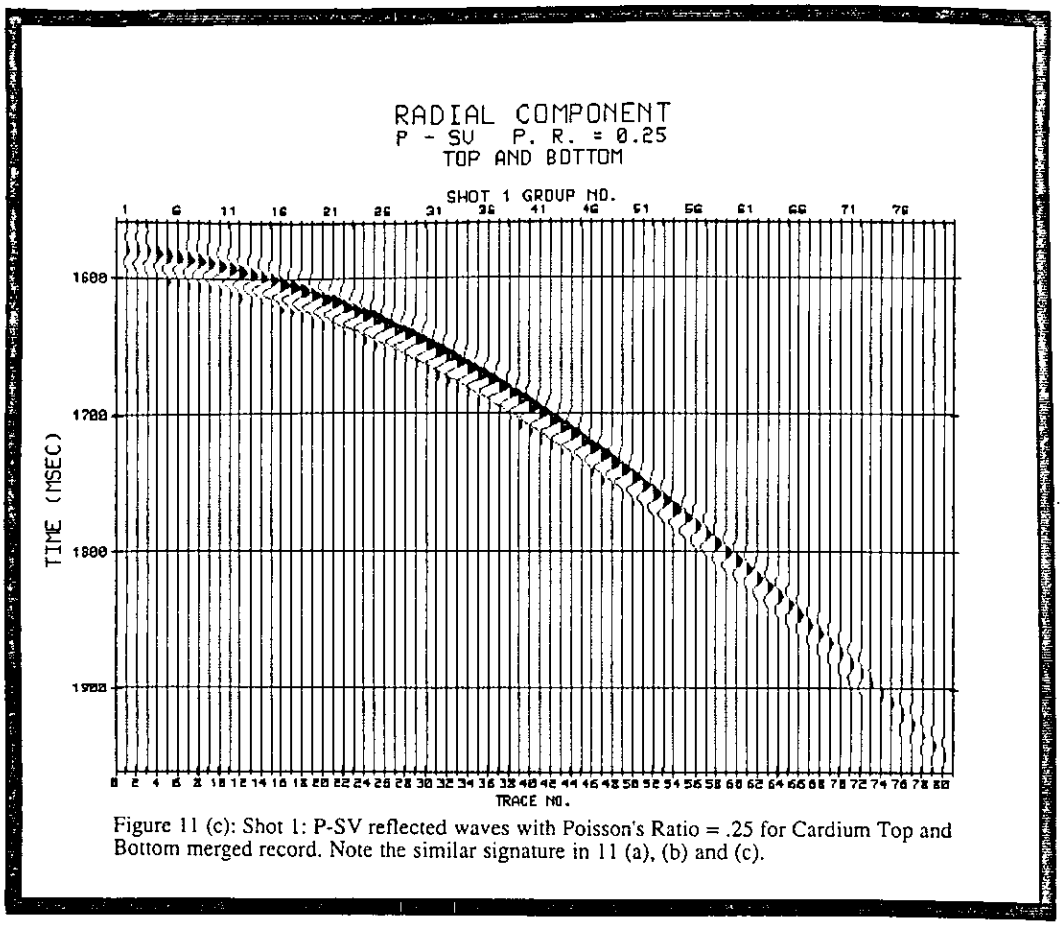

Figure 11 (c): Shot 1: P-SV reflected waves with Poisson's Ratio = .25 for Cardium Top and Bottom merged record. Note the similar signature in 11 (a), (b) and (c).

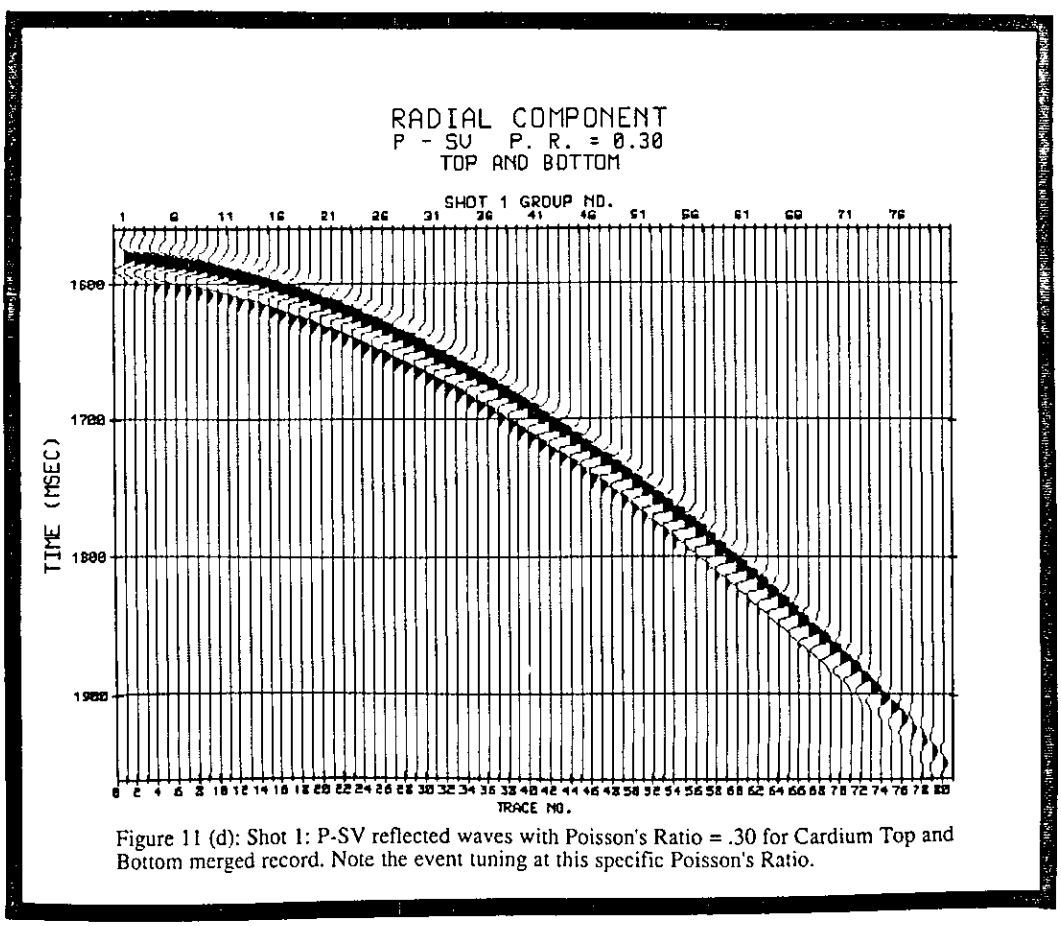

Figure 11 (d): Shot 1: P-SV reflected waves with Poisson's Ratio = .30 for Cardium Top and Bottom merged record. Note the event tuning at this specific Poisson's Ratio.

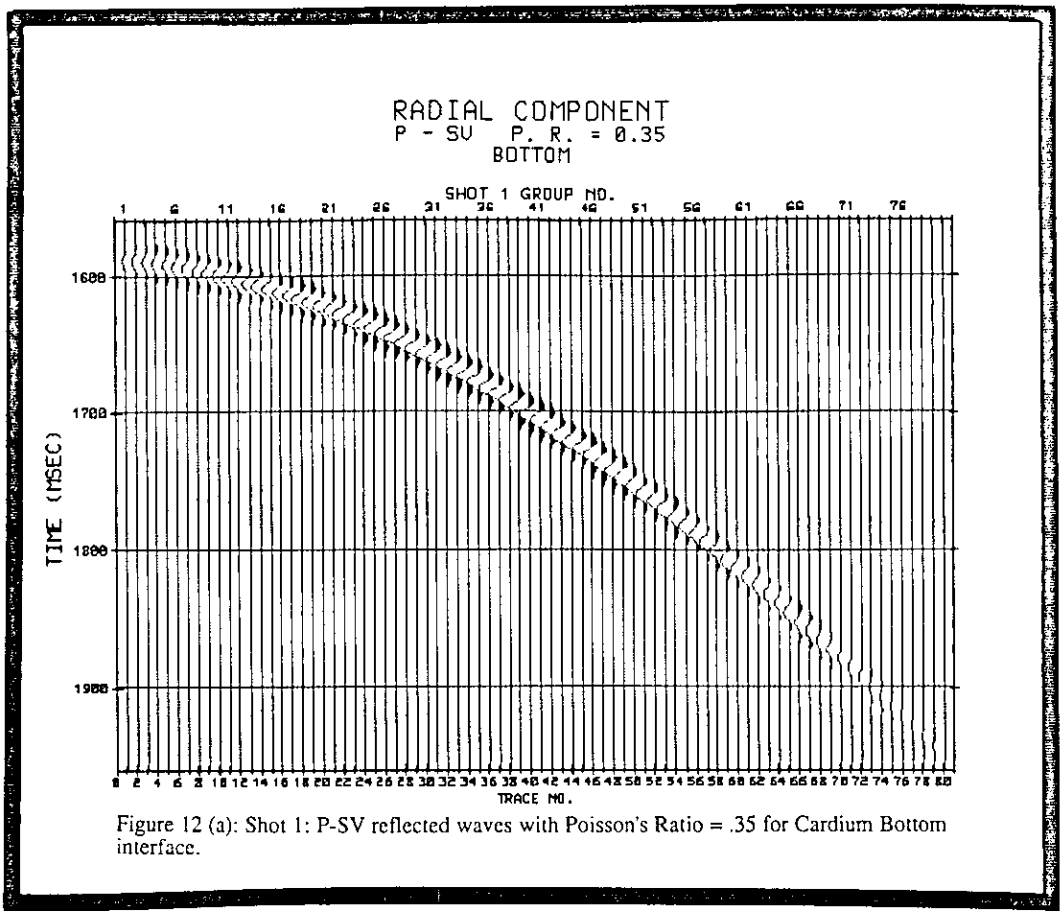

Figure 12 (a): Shot 1: P-SV reflected waves with Poisson's Ratio = .35 for Cardium Bottom interface.

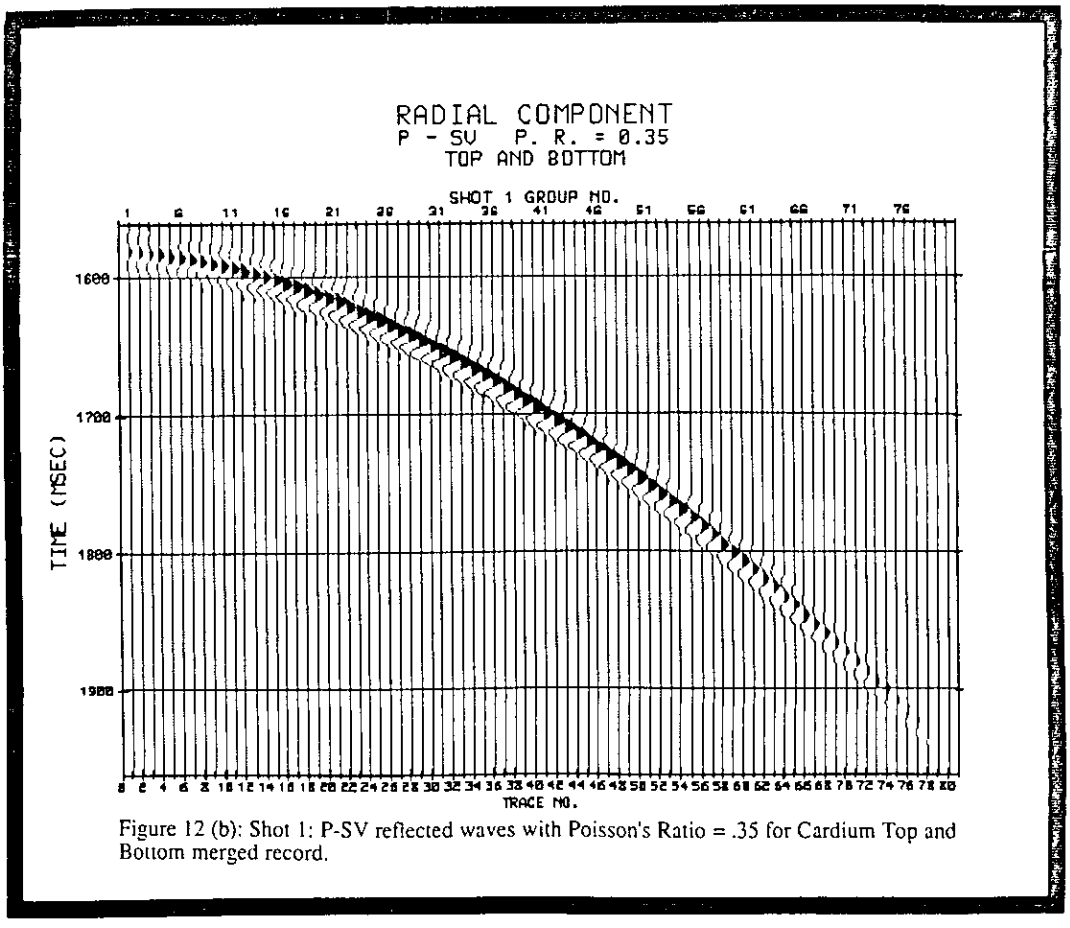

Figure 12 (b): Shot 1: P-SV reflected waves with Poisson's Ratio = .35 for Cardium Top and Bottom merged record.

To finalize our discussion, a last look at Figure 12 where $\sigma = .35$ shows that the Cardium event for the bottom boundary (Figure 12 (a)) does not contain the polarity reverse that the bottom interface used to exhibit for the other values of σ. In fact, a check with the computation program verified the polarity reverse occurrence but at larger offset than the maximum in shot 1 in that case. The top and bottom record (Figure 12 (b)) has almost the same signature as the corresponding record considered for constant $\sigma = .31$. This can be interpreted as the result of having $\sigma = .35$ while the surrounding media have $\sigma = .36$ in which case, reflections would be generated as these produced in the constant Poisson's ratio case.

CONCLUSIONS

In the case where Poisson's ratio is the same (or very close) in the two media bounded by the reflecting interface, the angle of incident has only minor effects on reflection coefficients over propagation angles commonly used in reflection seismology (precritical angle of incident). With substantial difference in Poisson's ratio across the interface, large changes in reflection coefficients are produced when considering different angle of incidence. Polarity change may occur in cases of different Poisson's ratio depending on the velocity contrast between the two media.

In thin-layer cases, resolution between boundary-reflected events is not always attainable. Even with different Poisson's ratios in one medium, subsurface boundaries can still give a similar signature. The case when Poisson's ratio is .30 (Cardium shear velocity of 2093 m/s) and Cardium thickness is 9 m, leads to event tuning.

REFERENCES

Aki., K., and Richards, P., 1980, Quantitative Seismology, **1**: W. H. Freeman and Co., 125-150.

Birch, F., Schairer, J. F., and Spicer, H. C., 1942, Handbook of physical constants: Geol. Soc. Am., Special Paper **36**

Chiburis, E. F., 1984, Analysis of Amplitude Versus Offset to detect Gas/Oil Contacts in the Arabian Gulf: Presented 54th Ann. Internat. Mtg., Soc. Expl. Geophys., Atlanta; abs., Geophysics, **50**, 344.

Garotta, R., 1987, Two-component acquisition as a routine procedure: Shear-wave Exploration; Soc. Expl. Geophys., 122-136.

Koefoed, O., 1955, On the effects of Poisson's ratios of rock strata on the reflection coefficients of plane waves: Geophys. Prosp., **3**, 381-387.

Muskat, M., and Meres, M. W., 1940, The seismic wave energy reflected from various types of stratified horizons: Geophysics, **5**, 149-155.

Ostrander, W. J., 1984, Plane-wave reflection coefficients for gas sands at nonnormal angles of incidence: Geophys., **49**, 1637-1648.

Swagor, N. S., 1975, The Cardium Conglomerate of the Carrot Creek Field, Central Alberta: Master Thesis, Department of Geology, The University of Calgary, p. 1.

Wood, R. A., 1979, Converted wave reflections in exploration seismic records: Presented 48th Ann. Internat. Mtg., Soc. Expl. Geophys., San Francisco; abs., Geophysics, **44**, 346.

Wren, A. E., 1984, Seismic techniques in Cardium exploration: J. Can. Soc. Expl. Geophys., **20**, 55-59.

Yilmaz, O., 1987, Seismic data processing: Soc. Expl. Geophys., 479-484.